

Fine-grained Visual Categorization using PAIRS: Pose and Appearance Integration for Recognizing Subcategories

Pei Guo
Brigham Young University
peiguo@cs.byu.edu

Ryan Farrell
Brigham Young University
farrell1@cs.byu.edu

Abstract

In Fine-grained Visual Categorization (FGVC), the differences between similar categories are often highly localized to a small number of object parts (see Figure 1), and significant pose variation therefore constitutes a great challenge for identification. To address this, we propose extracting image patches using pairs of predicted keypoint locations as anchor points. The benefits of this approach are two-fold: (1) it achieves explicit top-down visual attention on object parts (see Figure 5), and (2) the extracted patches are pose-aligned and thus contain stable appearance features. We employ the popular Stacked Hourglass Network [39] to predict keypoint locations, reporting state-of-the-art keypoint localization results on the challenging CUB-200-2011 [50] dataset. Anchored by these predicted keypoints, an overcomplete basis of pose-aligned patches is extracted and a specialized appearance classification network is trained for each patch. An aggregating network is then applied to combine the patch networks' individual predictions, producing a final classification score. Our PAIRS algorithm attains an accuracy of 88.6%, an increase of 1.1% over the current state-of-the-art. Enhancing the base PAIRS model with single-keypoint patches produces a further improvement, yielding a new state-of-the-art accuracy of 89.2% on the CUB dataset and clearly demonstrating the power of integrating pose and appearance features.

1. Introduction

Fine-grained visual categorization (FGVC) refers to the task of classifying subcategories within a basic-level category. Examples include: classifying bird species [48, 52] such as California Gull vs. Western Gull; discriminating dog breeds [26] such as Golden Retriever vs. Labrador Retriever; and, identifying car make and model [31, 55] such as Toyota Prius vs. Honda Insight. FGVC lies between generic category-level object recognition like the Imagenet challenge [42] and instance-level classification like

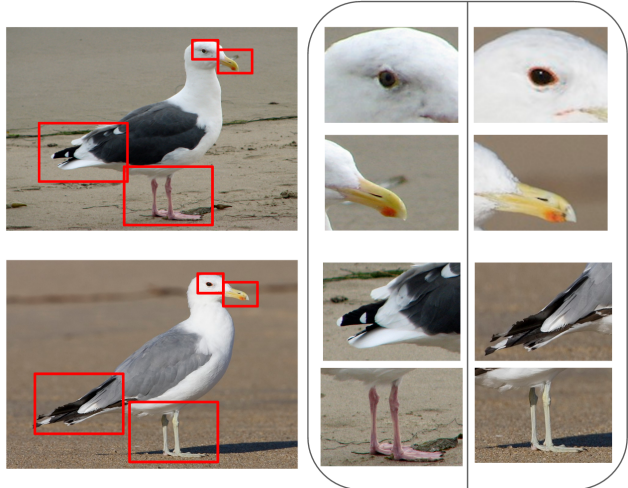


Figure 1. **Visually similar species with localized distinguishable parts.** This example shows how two similar species can be effectively classified by localized parts. The left half contains two images, a Western Gull (top) and a California Gull. The right half contains two columns, parts in the left column are from the Western Gull and those on the right are from the California Gull.

face recognition and other visual biometrics.

Fine-grained recognition can be extremely difficult for very similar species. Sometimes, the only clues available to separate such species lie in highly-localized patches. While a Western Gull and a California Gull both share a yellow bill, the former has just an orange spot on the end of the lower bill but the former has a black ring near the tip with a red spot on the underside. Another problem is that intraclass variance often exceeds interclass variance. Two images of the same bird species can look dramatically different if the birds have different poses. On the other hand, images of two different species within the same family can appear almost identical.

Fine-grained datasets tend to be modest in size. Gathering and correctly classifying such images requires extensive domain expertise which crowdsource workers cannot provide. It is difficult to accurately represent the distribution of



Figure 2. **Examples of pose aligned patch.** This example shows the back | right-eye patch for images from different classes. Pose-aligned patches isolate appearance from pose and are thus easier to classify.

possible images with only a few samples.

One promising direction in fine-grained recognition is the integration of pose and appearance information. This is usually done by dividing the object into pose-normalized appearance regions, each containing localized features. Previous part-based models define a part as a rectangular or square area around a keypoint. We refer to such parts as single keypoint patches. Methods leveraging single keypoint patches, such as [23, 58, 61], achieve a certain measure of success, however the number of the patches is greatly limited. Also, pose variation in the object will lead to part patches that are poorly-aligned.

We illustrate our algorithm pipeline in Figure 3. For keypoint detection, we employ the stacked hourglass network, which is first introduced in the human pose estimation domain. Maximum activation locations of the final layer feature maps are treated as the keypoint locations. Given the input image and detected keypoint locations, a rectangle bounding box around each keypoint pair is cropped and similarity-transformed to a uniform-sized patch (Figure 4), such that both keypoints are at fixed position across different images. For an object of N keypoints we have $\binom{N}{2}$ keypoint pairs. Patches generated in this way constitute a rich object representation effective at capturing pose-aligned appearance at different scales (Figure 5). As the representation is normalized to the keypoint locations, the patches are well-aligned, independent of the pose or the viewer's angle (see Figure 2). we train Resnet-50 networks as initial part classifiers. During part classifier training, all keypoints are considered visible. Eliminating patches with invisible keypoint will result in dataset shrinking and hurts model gen-

eralization (See Figure 10). We also consider object symmetry characteristics to further expand training set size and reduce overall model number. To aggregate part classifier scores, we explore different architectures based on the assumption that part contribution should be different for different images and classes. We find that Multi-Layer Perception (MLP), while being the most simple method, achieves the best final classification accuracy.

Deep neural networks are often treated like black boxes, with little knowledge of what is going on inside. Because the building blocks of our image representation are keypoint pair patches, our model enjoys an advantage over others that it is highly interpretable at patch level. We do thorough analysis for patch effectiveness comparison by per-patch predictions. We can also find hard cases by analyzing patch classification scores.

The core contribution of our approach, Pose and Appearance Integration for Recognizing Subcategories (PAIRS), is an automatic pipeline for estimating object pose and using keypoint pairs to extract pose-aligned patches. This strategy, subsequently combining the predictions from the pose-aligned patches, achieves state-of-the-art results on CUB-200-2011 [50]. The proposed approach constitutes a significant departure from recent research directions and hearkens back to pose-aligned patches first introduced by Berg *et al.* [1]. Leveraging the stacked hourglass network for pose estimation in the fine-grained domain, we achieved state-of-the-art keypoint localization on CUB-200-2011 [50]. We do thorough analysis on patch classification scores, unveiling interesting findings.

2. Related Work

2.1. Fine-grained Visual Categorization

Fine grained recognition has emerged as a new research interests in recent years. Early works include [11, 12, 37, 56, 57, 59, 60]. With the roaring success in large-scale image classification [10, 32], the Convolutional Neural Networks (CNNs) [34] have been applied to various domains including general object classification [21, 22, 46, 47], object detection [18, 19, 20, 40, 41] and semantic segmentation [6, 45]. Fine-grained visual categorization has also witnessed the wide adoption of CNN-based approaches. Among these approaches, several directions have shown promise and have achieved strong results. A brief introduction along with some representative work follows.

Part-based models. Decomposing the object into informative parts dates back to deformable part models and its extinctions [2, 12, 13]. In fine grained recognition, examples include [3, 23, 28, 58, 61, 35]. [58] first employs R-CNN [18] for whole-object and part detection. [24] propose to do keypoint detection using fully convolutional networks [45]. [61] introduces an end-to-end learning frame-

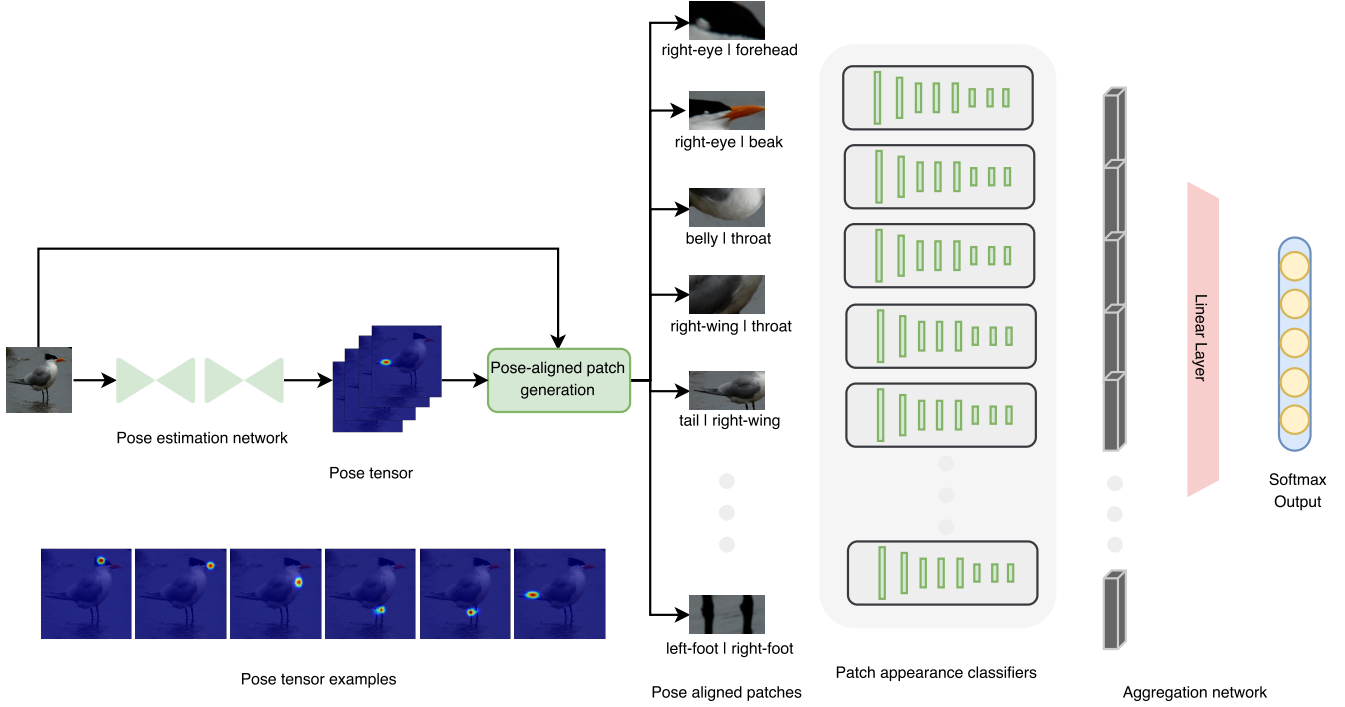


Figure 3. Overview of the Proposed Framework for Fine-grained Recognition. We first apply a pose estimation network to the image for keypoint detection. Pose-aligned patches are then extracted from the image using the predicted keypoint locations. We then do fine-grained prediction on the individual patches using patch specific networks. These per-patch predictions are concatenated and fed into an aggregation network for the final fine-grained classification.

work for pose estimation, normalization and recognition. Although related to our method, these frameworks usually utilize less patches than ours and lack pose alignment.

Attention-based models. Attention mechanisms work by guiding the CNN to sequentially focus on selective parts of the whole image. Human vision works in a similar way, first glancing at the whole object then attending to small important regions. Works along this direction include [14, 33, 38, 43, 53, 63]. [33] proposes unifying new patch candidates and informative part evaluation with long short term memory networks (LSTM), and fusing all proposals for final recognition. This work establishes the current state-of-the-art performance on CUB-200-2011 [52] dataset, achieving 87.5% accuracy with part annotations.

Feature correlation and kernel mapping. [36] proposes a simple yet effective bilinear pooling layer to compute a second order polynomial kernel mapping on CNN features. Some approaches extend bilinear pooling. Compact bilinear pooling [15] proposes a compact representation to approximate the polynomial kernel, reducing memory usage. Low-rank bilinear pooling [27] represents the covariance features as a matrix and applies a low-rank bilinear classifier. Kernel pooling [9] proposes a general pooling framework that captures higher order interactions of features in the form of kernels.

Human-in-the-loop. Human-in-the-loop refers to the

efforts to interactively combine human knowledge in a computational algorithm. Representative works include [4, 5, 8, 49]. Human-in-the-loop has been shown effective for dataset collection and interactive recognition.

Alignment. Unlike previous papers which rely on detectors for part localization, [16, 17] propose to localize distinctive details by roughly aligning the objects using just the overall shape. Spatial Transformer Networks [25] propose a differentiable layer for learning affine transformation parameters and conducting image transformation. This layer can be inserted anywhere and shows promise in the fine-grained recognition domain.

Perhaps the work most relevant to ours is Berg *et al.*'s Part-based One-vs-One Features (POOF) [1]. While our treatment also builds on patches derived from keypoint pairs, we differ in the following aspects: 1) Our patch extraction and classifier are both based on convolutional neural networks and achieve state-of-the-art keypoint prediction and classification result on CUB-200-2011. 2) We use multi-class based classifiers while POOF uses one-versus-all SVM classifiers.

We note that Krause, *et al.* [30] achieved the highest accuracy on the CUB dataset at 92.3%. However, few works consider or include this work in comparisons as the technique leveraged thousands of noisy-labeled training images outside of the dataset itself.

2.2. Human pose estimation

Human pose estimation, which refers to the task of localizing human body joints, has seen increasing attention in the vision community. Our keypoint detection is closely related to this field of research, however, a complete survey is beyond the scope of this paper. Several recent developments are discussed below.

[51] designs a sequential architecture composed of convolutional networks that directly operate on belief maps from previous stages, producing increasingly refined estimates for part locations without explicit graphical model-style inference. In [39], Features are processed across all scales and consolidated to best capture the various spatial relationships associated with the body. The repeated bottom-up, top-down processing used in conjunction with intermediate supervision is critical to improving the performance of the network. State-of-the-art results are achieved on the FLIC and MPII benchmarks. [7] employs adversarial training for learning pose priors, building on top of generative adversarial networks (GAN).

3. PAIRS - Pose and Appearance Integration

PAIRS, the proposed approach, contains three major components: (1) a pose estimation network for keypoint detection followed by off-line patch cropping; (2) a patch classification network for feature extraction; (3) a feature aggregation network for combining patch features and producing final fine-grained prediction. Unlike previous part-based models [23, 58, 61], which only deal with single keypoint crops, PAIRS extracts pose-aligned patches with diverse combinations of two keypoints.

3.1. Pose Estimation Network

Pose estimation networks usually follow one of two paradigms for prediction. One is to directly regress to discrete keypoint coordinates in the form $(x_i, y_i), i \in \{1, \dots, P\}$ with P being the number of keypoints. Fully convolutional network and variants, would instead describe the keypoint location as a probability distribution on the whole image. A $P \times H \times W$ pose tensor is associated with each image for training. Each channel of the pose tensor represents the probability distribution of certain keypoint. The ground truth keypoint mapping is often treated as a Gaussian distribution centered on the true keypoint location.

The stacked hourglass network (SHN) produces this second type prediction using heat maps as the target. The SHN consists of multiple hourglass-shaped subnetworks; each hourglass subnetwork is a sequence of several bottom-up top-down convolutional layers. Pooling layers are used to down-sample the feature size and to extract high level semantic information. Upsampling layers are used to boost feature map resolution, providing more detailed and local-

ized information. Skip layers are added within each building block to help train when the network goes deeper. The output of the stacked hourglass is a 15 -channel pose tensor, each channel representing the probability distribution of a certain keypoint. Supervision is added after each hourglass subnetwork for faster training convergence.

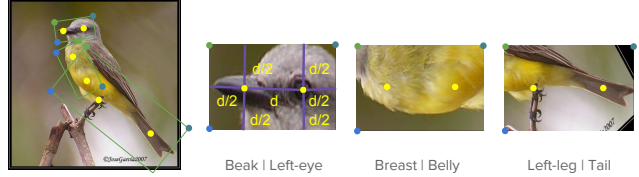


Figure 4. **Similarity transform for keypoint pair patch.** Similarity transform is performed to extract keypoint patches from the original image. Only scaling, rotation and translation are used during the transformation. The distances between the two keypoints and the border of image are given in the `beak | left-eye` example.

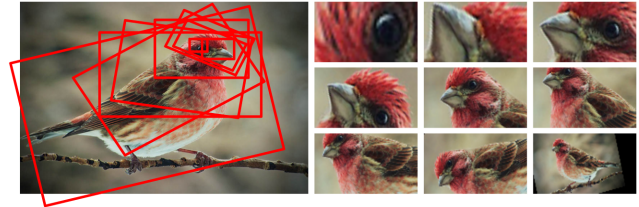


Figure 5. **Range of keypoint pair patches.** We show the spectrum of generated patches. Patches are of different sizes and capture different areas spread across the bird's body.

3.2. Patch Generation and Patch-Level Prediction

Based on the keypoint locations predicted by the Pose Estimation Network, diverse pose-aligned patches, each anchored by two keypoints, are generated from every image. Consider, for example, the `left-eye | beak` patch. In a given image, the predicted locations of the `left-eye` and the `beak` are used to compute a similarity transformation that is used to extract a pose-aligned patch such as those shown in Figure 2. The pose-aligned patch representation aligns the respective keypoints in a keypoint pair, effectively normalizing them to the same location in all extracted patches.

Utilizing the set of extracted image patches for a given `A | B` patch, a Patch Classification Network is trained for that patch. The trained network takes a patch as input and produces an independent prediction of the fine-grained category for the image that the patch came from. We use the class predictions generated by the Patch Classification Network as the feature describing a patch. Concatenating the predictions of all 105 patches, we obtain a $105 \times 200 = 21,000$ -dimensional feature vector. Note that 200 is dataset

specific. Alternately, the activations from the final convolutional layer of the network could also be used as a patch description.

Symmetry. Symmetry is a useful characteristic, both for increasing training data and for model simplification. A bird exhibits bilateral symmetry, and thus has left/right pairs of eyes, wings and feet.

When training part classification models, we treat each symmetric keypoint pair (eyes/wings/feet) as a single keypoint, merging *e.g.* two patches into a single *hybrid* patch. This reduces the number of distinct patches for the 15 keypoints from 105 to 69. We then train a separate CNN model for each hybrid patch. At inference stage, we apply hybrid patch model to each original patch, so we still have 105 patch representations for each image. We observe consistent patch accuracy increase after applying symmetry to the dataset.

Visibility. Due to self-occlusion and foreground-occlusion, usually some keypoints are missing from the image. One way to deal with keypoint invisibility is to only keep those patches with pairs of visible keypoints. This will result in the reduction of training set size and affect the patch classifier negatively. We instead treat all keypoints as visible and take the maximum activation point as the keypoint location. Although our method will yield some noisy patches, our patch classifiers actually get better accuracy using this strategy (Figure 10). Reasons for this include: (1) we enjoy a larger training set, and (2) the pose estimation network will make a reasonable guess even if certain keypoints are missing.

3.3. Patch Aggregation Network

Our method has a rich and explicit part based representation for an image. To aggregate the part representations we explored the following directions.

Average of Best K Patches. A basic assumption in fine grained recognition is that only a few patches are important for the final decision, and other patches may act as noise and hurt performance. We propose a patch selection scheme to find top K patch with highest average score. A greedy search algorithm would work as follows: for each of the K combination, the K patch average score is computed as the final image score. The complexity for this algorithm is $\sum_{K=1}^{105} \binom{105}{K}$. The number of combinations to search grows in the order of $K!$ and quickly becomes intractable, for example after only 5 iterations the patch number goes to $\binom{105}{5} = 9.65 \times 10^7$. We thus employ the *beam search* algorithm. For each round of training, we only keep top 100 patch combinations as the seeds. We will not greedily search the whole parameter space but only build our search path on the basis of the previous 100 patch combinations. Two variants of the beam search algorithm are tried. One is to find best patch combination on training set and test it on

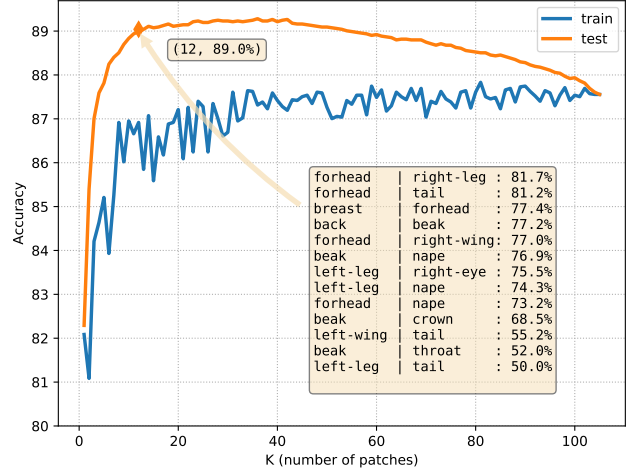


Figure 6. **Selecting the best K patches.** For the blue curve, we use beam search algorithm on the training set, trying to find the best set of K patches and plot that set's performance on the testing set. The testing accuracy plateaus after around 10 patches, because patches that work well on the training set don't necessarily generalize well to the testing set. The orange curve, on the other hand, uses the beam search directly on testing set for training and testing. This experiment reveals the potential of a small set of patches. If regularized well, beam search can reach well above 89%. In the inset, we show a list of the 12 patches attaining 89% accuracy. The selected patches range from the whole body to localized parts.

testing set. The blue curve in Figure 6 shows how testing accuracy change with respect to the patch number K . We also search top K patches on the testing set. This operation, although invalid, provides some insights in the potential of this method. The orange curve shows the testing accuracy with respect to the patch number K . It is well above the 89% line on a series of K values. Figure 6 also shows that patches performs best on training set does not guarantee consistent performance on testing set, and if we can find good regularization approach, the testing accuracy can be higher than 89% with the beam search algorithm.

Sparingly Gated Network. As an alternative method, partially inspired by [44], we experiment with the sparsely gated network for model aggregation. The motivation is that we need to dynamically select patches so that for different images, different sets of patches are used towards final classification. The beam search algorithm mentioned above will have fixed patch weight across the whole dataset. Our gated network consists of a tiny neural network whose output consists the weights for 105 patches. We then impose an explicit sparsity constraint on the output of the gated network to only allow the top K patches to have non-zero values. The rest are set to negative infinity. A Sigmoid layer is added to transform the K weight between 0 and 1. The network architecture is described below.

$$G(x) = \text{Softmax}(\text{KeepTopK}(H(x), K))$$

We tried different settings for the gated network and find a simple linear layer would work decently most of the time. We conduct the experiment to do grid search for optimal result with respect to the hyper parameter K. We find actually when K=105, the accuracy achieves the highest accuracy of 87.2%. This experiment is purely for estimating the potential of the sparsely gated network.

An interesting case here is when K=1. We select only one patch for each image and use the patch score as the final classification score. The proposed network obviously fails to find the best patch. We know that some patches alone can get 80+% accuracy. So even if the gated network selects the same patch for every image, the potential accuracy should be well above 80%. We guess the reason behind is the gated network in our case does not learn useful information in order to make decision on which patch are relatively more important.

LSTM Network. As the third experiment, we tried recurrent neural networks (RNN) for patch selection. RNN enjoys the advantage of sequentially focusing on different part of the image remember previous states within its hidden layer. We use a one layer LSTM(Long Short Term Memory) with 512 nodes. Each has a hidden layer of size 1024. The last output of sequence is selected as the final output. We get 82.7% in this experiment. This confirms the effectiveness of the LSTM network.

Multiple Layer Perceptron. The final and most effective method we tried is vanilla MLP network. The MLP network contains one hidden layer with 1024 parameters, followed by the batch normalization layer, ReLU layer, and then the output layer. With 105 patch pairs, our final accuracy is 88.6% , 1.1% higher than the current state-of-the-art result.

4. Experimental Evaluation

We test our algorithm on CUB-200-2011 dataset. This is a challenging dataset with 200 species of birds. There are 5994 training images and 5794 testing images. Class labels and keypoint locations are provided in the original dataset.

We employ Torch7 as our code framework. Our stacked hourglass network consists of two hour-glass submodules. the input is color normalized and uniformly resized to 256×256 . Random rotation and flipping are used as data augmentation. The rotation angles include $\{0, 90, 180, 270\}$. Improvement observed with these preprocessing step. Batch size is 8 and the memory consumption is about 6GB. Output is boosted from 64x64 to 256x256 for better accuracy on a finer resolution. We train 100 epochs on the GeForce GTX 1080Ti for 5 hours. The initial learning rate is 0.001 and drops by a factor of 10 every 30 epochs. The total epoch is 100. We train the network from scratch without fine tuning. Experiments show very low generalization error.

During the training process for patch classifiers, batch size is set to 16 and the memory consumption is about 4GB.

Table 1. PCK comparison

Name	Huang[23]	Zhang [61]	Ours
back	80.7	85.6	92.46
beak	89.4	94.9	97.96
belly	79.4	81.9	89.02
breast	79.9	84.5	92.27
crown	89.4	94.8	97.61
forehead	88.5	96.0	98.20
left-eye	85.0	95.7	98.21
left-leg	75.0	64.6	86.02
left-wing	67.0	67.8	81.05
nape	85.7	90.7	95.55
right-eye	86.1	93.8	98.04
right-leg	77.5	64.9	85.92
right-wing	67.8	69.3	80.94
tail	76.0	74.7	86.60
throat	90.8	94.5	97.85
Overall	86.6	-	92.39

Initial learning rate is 0.001 and drops by a factor of 10 after every 30 epochs. It takes about 50 minutes to train each model for 50 epochs.

For the MLP, we train for 50 epochs with initial learning 0.001 and drops every 30 epochs at the factor of 0.1.

4.1. Keypoint prediction performance

We use PCK (Percentage of Correct Keypoints) score to measure the accuracy of keypoint prediction results. If a keypoint is predicted to be within a small distance $a * \max(h, w)$ away from the ground truth location then it counts as a correct predict keypoint. Usually $a = 0.1$, $\max(h, w)$ is the bigger value between the bounding box height and width. Our result along with some other baseline models are shown in Table 1. We achieve highest score on all 15 keypoints with considerable leading margin. We do especially well on legs and wings where other models struggle to make precise prediction.

Although we localize wings and legs better than baselines, they still have the lowest PCK in our model. This is caused by dramatic pose change as well as the appearance similarity between symmetric parts. We note that using keypoints to denote the wings is not always appropriate. Because wings are 2D shaped parts that spread over a relatively large area on the image. Designating a keypoint to the wing can be obscure, because it is not easy to decide which point represents the wing location better. In fact, the ground truth keypoint location of the CUB dataset is the average of five annotators' results. Those human generated annotations often disagree with each other.

4.2. Classification

Throughout our experiments, we have used the ResNet-50 architecture as the patch classification network due to its



Figure 7. **Examples of Keypoint Detection using the Stacked Hourglass Network [39].** The red dots represent the predicted keypoint locations while the black dots indicate the ground truth keypoint locations. The bottom row shows some failure cases. Most of these failures confuse the left and right wings or the left and right legs. We suspect this is caused by a combination of less frequent poses and visual similarity between symmetric parts. In the last image of the bottom row the reflect in the water is believed to be the tail.

Table 2. **Classification score on CUB.** Annotation key as follows: GT = class labels; BB = bounding box annotation; parts = keypoint annotations; web = images downloaded from the Internet.

Method	Annotations used	Accuracy
Huang <i>et al.</i> [23]	GT+BB+parts	76.2
Zhang <i>et al.</i> [58]	GT + BB	76.4
Krause <i>et al.</i> [29]	GT+BB	82.8
Jaderberg <i>et al.</i> [25]	GT	84.1
Shu <i>et al.</i> [27]	GT	84.2
Zhang <i>et al.</i> [62]	GT	84.5
Xu <i>et al.</i> [54]	GT+BB+parts+web	84.6
Lin <i>et al.</i> [36]	GT+BB	85.1
Cui <i>et al.</i> [9]	GT	86.2
Lam <i>et al.</i> [33]	GT+parts	87.5
PAIRS Only	GT + parts	88.6
PAIRS+Single	GT + parts	89.2

high performance despite its compact GPU footprint. For the ResNet-50 network, the penultimate (the final convolutional) layer produces a 2048-dimensional vector. We find in our experiments that this 2048-dimensional feature does

not lead to better performance than 200-dimensional class prediction vector. Alternate architectures to the ResNet-50 can easily be adapted.

Our pairs representation alone produces 88.6% accuracy. We combine pairs patch with single keypoint patch and achieves a new state-of-the-art 89.2% accuracy. We compared our result with several other strong baselines in Table-2. For many years, performance in fine-grained recognition has been largely evaluated on the CUB-200 dataset. After the dataset was released, performance climbed steadily for several years, yet increases may be tapering off. Many techniques in the last couple of years have successfully achieved performance in the range of 84-86% accuracy, but there are indications that this may be a plateau. Our algorithm shows the pairs representation is promising and can achieves superior result compared to others.

4.3. Results Visualization

Given 105 patches on one image, we are interested to know how prediction accuracy is distributed across the patches. We show the patch effectiveness histogram in Fig-

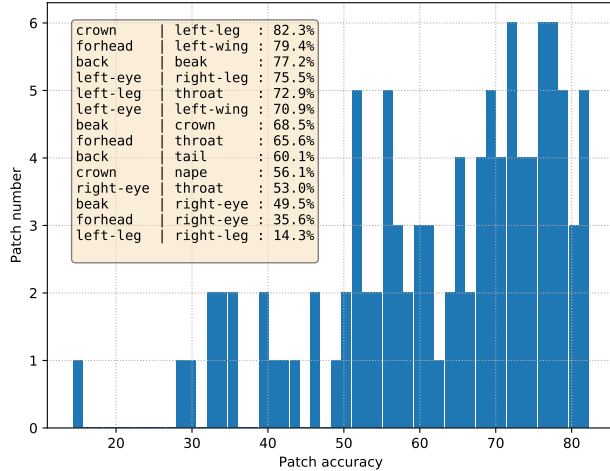


Figure 8. **Patch Effectiveness Histogram.** This histogram shows statistics about how individual patch classifiers perform. Different patches have different classification potential. In the inset we show a sampling of patches with accuracy from highest and lowest. Larger patches usually performs better than small ones, but small patch also contribute to the final accuracy in critical case (Figure 6).

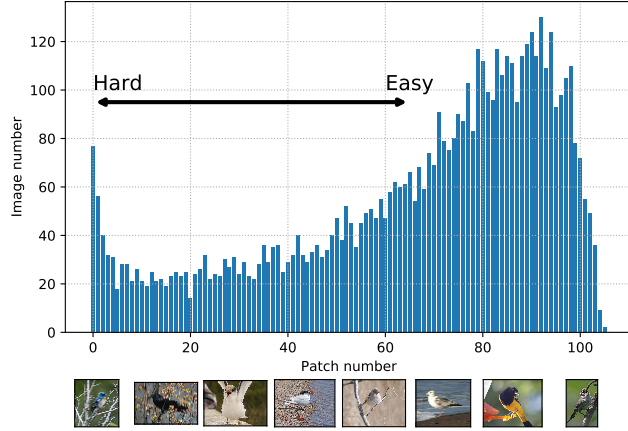


Figure 9. **Image Difficulty Measure.** This figure shows, for each image, how many of its patches can *independently* classify it correctly. If few patches can produce a correct classification score, then the image is a difficult one. We show some sample images from hard to easy at the bottom of the figure. Note the increasingly cluttered backgrounds of the more difficult images.

ure 8. We notice there is one patch does extremely poorly, only achieving 14.3% accuracy. This patch corresponds to the `left-leg | right-leg` pair.

We also identify hard cases by patch score. If an image can be classified correctly by most of its patches, then it belongs to the easy category. Otherwise, it belongs to hard case category. The image difficulty distribution is shown in Figure 9. This figure also provides sample images ranging from hard to easy. Note the increasingly cluttered back-

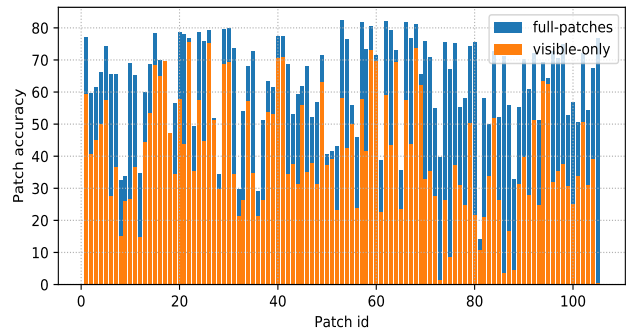


Figure 10. **Effect of invisible keypoint patch elimination.** We show here the testing accuracy of each patch with and without invisible keypoint patch elimination. The blue bars represent patches generated by predicted keypoints (including every keypoint pair patch). The orange bars represent patches generated by only visible keypoints.

Table 3. **Patch Size Impact on Patch Classification Network**
Test accuracy for the `crown | left-leg` patch with different patch size. Note that no symmetry augmentation is used.

Patch Size	Accuracy
32×64	60.0
64×128	74.5
128×256	79.6
256×512	80.6

ground towards the difficult end.

4.4. Patch Size Study

Patch size is an important hyper parameter in our experiment. To study its affect on the patch classifier accuracy, we choose the `crown | left-leg` patch and run ResNet-50 on 4 different sizes of input. Results are shown in Table 3. We find generally larger patch will get better accuracy score. We choose 256×512 also because our ResNet-50 models are pretrained on such resolution on ImageNet dataset.

5. Conclusion

In this paper, we introduce the PAIRS framework for fine-grained recognition, which is composed of pose estimation, pose-aligned patch extraction and patch score aggregation. We achieve state-of-the-art accuracy on the CUB-200-2011 dataset. Our pose estimation network also attains state-of-the-art PCK on the CUB-200-2011 dataset. The keypoint pair patches constitute a rich object representation effective at capturing pose-aligned appearance at different scales. The proposed approach shows that the integration of pose and appearance is a promising direction for further exploration.

References

- [1] T. Berg and P. N. Belhumeur. POOF: Part-Based One-vs.-One Features for Fine-Grained Categorization, Face Verification, and Attribute Estimation. In *CVPR*, 2013. 2, 3
- [2] L. Bourdev and J. Malik. Poselets: Body part detectors trained using 3D human pose annotations. In *ICCV*, 2009. 2
- [3] S. Branson, G. Van Horn, P. Perona, and S. Belongie. Bird Species Recognition Using Pose Normalized Deep Convolutional Nets. In *BMVC*, 2014. 2
- [4] S. Branson, G. Van Horn, C. Wah, P. Perona, and S. Belongie. The Ignorant Led by the Blind: A Hybrid Human-Machine Vision System for Fine-Grained Categorization. *IJCV*, 108(1):3–29, 2 2014. 3
- [5] S. Branson, C. Wah, F. Schroff, B. Babenko, P. Welinder, P. Perona, and S. Belongie. Visual Recognition with Humans in the Loop. In *ECCV*. 2010. 3
- [6] L.-C. Chen, G. Papandreou, I. Kokkinos, K. Murphy, and A. L. Yuille. Deeplab: Semantic image segmentation with deep convolutional nets, atrous convolution, and fully connected crfs. *arXiv preprint arXiv:1606.00915*, 2016. 2
- [7] Y. Chen, C. Shen, X.-S. Wei, L. Liu, and J. Yang. Adversarial PoseNet: A Structure-aware Convolutional Network for Human Pose Estimation. *arXiv preprint arXiv:1705.00389*, 2017. 4
- [8] Y. Cui, F. Zhou, Y. Lin, and S. Belongie. Fine-Grained Categorization and Dataset Bootstrapping Using Deep Metric Learning With Humans in the Loop. In *CVPR*, 2016. 3
- [9] Y. Cui, F. Zhou, J. Wang, X. Liu, Y. Lin, and S. Belongie. Kernel Pooling for Convolutional Neural Networks. In *CVPR*, 2017. 3, 7
- [10] J. Deng, W. Dong, R. Socher, L.-J. Li, K. Li, and L. Fei-Fei. ImageNet: A large-scale hierarchical image database. In *CVPR*, 2009. 2
- [11] K. Duan, D. Parikh, D. Crandall, and K. Grauman. Discovering localized attributes for fine-grained recognition. In *CVPR*, 2012. 2
- [12] R. Farrell, O. Oza, V. I. Morariu, N. Zhang, T. Darrell, and L. S. Davis. Birdlets: Subordinate categorization using volumetric primitives and pose-normalized appearance. In *ICCV*, 2011. 2
- [13] P. F. Felzenszwalb, R. B. Girshick, D. McAllester, and D. Ramanan. Object detection with discriminatively trained part-based models. *PAMI*, 32(9):1627–45, 9 2010. 2
- [14] J. Fu, H. Zheng, and T. Mei. Look Closer to See Better: Recurrent Attention Convolutional Neural Network for Fine-Grained Image Recognition. In *CVPR*, 2017. 3
- [15] Y. Gao, O. Beijbom, N. Zhang, and T. Darrell. Compact Bilinear Pooling. In *CVPR*, 2016. 3
- [16] E. Gavves, B. Fernando, C. Snoek, A. Smeulders, and T. Tuytelaars. Fine-Grained Categorization by Alignments. In *ICCV*, 2013. 3
- [17] E. Gavves, B. Fernando, C. G. M. Snoek, A. W. M. Smeulders, and T. Tuytelaars. Local Alignments for Fine-Grained Categorization. *IJCV*, 111(2):191–212, 2015. 3
- [18] R. Girshick. Fast R-CNN. In *CVPR*, 2015. 2
- [19] R. Girshick, J. Donahue, T. Darrell, and J. Malik. Rich Feature Hierarchies for Accurate Object Detection and Semantic Segmentation. In *CVPR*, 2014. 2
- [20] K. He, G. Gkioxari, P. Dollár, and R. Girshick. Mask R-CNN. In *ICCV*, 2017. 2
- [21] K. He, X. Zhang, S. Ren, and J. Sun. Deep Residual Learning for Image Recognition. In *CVPR*, 2016. 2
- [22] G. Huang, Z. Liu, and K. Q. Weinberger. Densely Connected Convolutional Networks. *CVPR*, 2017. 2
- [23] S. Huang, Z. Xu, D. Tao, and Y. Zhang. Part-Stacked CNN for Fine-Grained Visual Categorization. In *CVPR*, 2016. 2, 4, 6, 7
- [24] S. Huang, Z. Xu, D. Tao, and Y. Zhang. Part-stacked cnn for fine-grained visual categorization. In *The IEEE Conference on Computer Vision and Pattern Recognition (CVPR)*, June 2016. 2
- [25] M. Jaderberg, K. Simonyan, A. Zisserman, and K. Kavukcuoglu. Spatial Transformer Networks. In *NIPS*, 2015. 3, 7
- [26] A. Khosla, N. Jayadevaprakash, B. Yao, and L. Fei-Fei. Novel dataset for Fine-Grained Image Categorization. In *CVPR Workshops (FGVC)*, 2011. 1
- [27] S. Kong and C. C. Fowlkes. Low-rank Bilinear Pooling for Fine-Grained Classification. In *CVPR*, 2017. 3, 7
- [28] J. Krause, T. Gebru, J. Deng, L. J. Li, and L. Fei-Fei. Learning Features and Parts for Fine-Grained Recognition. In *ICPR*, 2014. 2
- [29] J. Krause, H. Jin, J. Yang, and L. Fei-Fei. Fine-Grained Recognition without Part Annotations. In *CVPR*, 2015. 7
- [30] J. Krause, B. Sapp, A. Howard, H. Zhou, A. Toshev, T. Duerig, J. Philbin, and L. Fei-Fei. The Unreasonable Effectiveness of Noisy Data for Fine-Grained Recognition. In *ECCV*, 2016. 3
- [31] J. Krause, M. Stark, J. Deng, and L. Fei-Fei. 3D Object Representations for Fine-Grained Categorization. In *ICCV Workshops (3DRR)*, 2013. 1
- [32] A. Krizhevsky, I. Sutskever, and G. E. Hinton. ImageNet Classification with Deep Convolutional Neural Networks. In *NIPS*, 2012. 2
- [33] M. Lam, B. Mahasseni, and S. Todorovic. Fine-Grained Recognition as HSnet Search for Informative Image Parts. In *CVPR*, 2017. 3, 7
- [34] Y. LeCun, L. Bottou, Y. Bengio, and P. Haffner. Gradient-based learning applied to document recognition. *Proceedings of the IEEE*, 86(11):2278–2324, 1998. 2
- [35] D. Lin, X. Shen, C. Lu, and J. Jia. Deep lac: Deep localization, alignment and classification for fine-grained recognition. In *2015 IEEE Conference on Computer Vision and Pattern Recognition (CVPR)*, pages 1666–1674, June 2015. 2
- [36] T.-Y. Lin, A. RoyChowdhury, and S. Maji. Bilinear CNN Models for Fine-Grained Visual Recognition. In *ICCV*, 2015. 3, 7
- [37] J. Liu, A. Kanazawa, D. W. Jacobs, and P. N. Belhumeur. Dog Breed Classification Using Part Localization. In *ECCV*, 2012. 2

[38] X. Liu, J. Wang, S. Wen, E. Ding, and Y. Lin. Localizing by Describing: Attribute-Guided Attention Localization for Fine-Grained Recognition. In *AAAI*, 2017. 3

[39] A. Newell, K. Yang, and J. Deng. Stacked Hourglass Networks for Human Pose Estimation. In *ECCV*, 2016. 1, 4, 7

[40] J. Redmon, S. Divvala, R. Girshick, and A. Farhadi. You only look once: Unified, real-time object detection. In *CVPR*, 2016. 2

[41] S. Ren, K. He, R. Girshick, and J. Sun. Faster R-CNN: Towards real-time object detection with region proposal networks. In *NIPS*, 2015. 2

[42] O. Russakovsky, J. Deng, H. Su, J. Krause, S. Satheesh, S. Ma, Z. Huang, A. Karpathy, A. Khosla, M. Bernstein, A. C. Berg, and L. Fei-Fei. ImageNet Large Scale Visual Recognition Challenge. *IJCV*, 115(3):211–252, 12 2015. 1

[43] P. Sermanet, A. Frome, and E. Real. Attention for Fine-Grained Categorization. In *ICLR*, 2015. 3

[44] N. Shazeer, A. Mirhoseini, K. Maziarz, A. Davis, Q. V. Le, G. E. Hinton, and J. Dean. Outrageously large neural networks: The sparsely-gated mixture-of-experts layer. *CoRR*, abs/1701.06538, 2017. 5

[45] E. Shelhamer, J. Long, and T. Darrell. Fully Convolutional Networks for Semantic Segmentation. *PAMI*, 39(4):640–651, 4 2017. 2

[46] K. Simonyan and A. Zisserman. Very Deep Convolutional Networks for Large-Scale Image Recognition. In *ICLR*, 2015. 2

[47] C. Szegedy, W. Liu, Y. Jia, P. Sermanet, S. Reed, D. Anguelov, D. Erhan, V. Vanhoucke, and A. Rabinovich. Going deeper with convolutions. In *CVPR*, 2015. 2

[48] G. Van Horn, S. Branson, R. Farrell, S. Haber, J. Barry, P. Ipeirotis, P. Perona, and S. Belongie. Building a Bird Recognition App and Large Scale Dataset With Citizen Scientists: The Fine Print in Fine-Grained Dataset Collection. In *CVPR*, 2015. 1

[49] C. Wah, S. Branson, P. Perona, and S. Belongie. Multiclass recognition and part localization with humans in the loop. In *ICCV*, 2011. 3

[50] C. Wah, S. Branson, P. Welinder, P. Perona, and S. Belongie. The Caltech-UCSD Birds-200-2011 Dataset. Technical report, California Institute of Technology, 2011. 1, 2

[51] S.-E. Wei, V. Ramakrishna, T. Kanade, and Y. Sheikh. Convolutional Pose Machines. In *CVPR*, 2016. 4

[52] P. Welinder, S. Branson, T. Mita, C. Wah, F. Schroff, S. Belongie, and P. Perona. Caltech-UCSD Birds 200. Technical Report CNS-TR-2010-001, California Institute of Technology, 2010. 1, 3

[53] T. Xiao, Y. Xu, K. Yang, J. Zhang, Y. Peng, and Z. Zhang. The Application of Two-Level Attention Models in Deep Convolutional Neural Network for Fine-Grained Image Classification. In *CVPR*, 2015. 3

[54] Z. Xu, S. Huang, Y. Zhang, and D. Tao. Augmenting Strong Supervision Using Web Data for Fine-Grained Categorization. In *ICCV*, 2015. 7

[55] L. Yang, P. Luo, C. C. Loy, and X. Tang. A Large-Scale Car Dataset for Fine-Grained Categorization and Verification. In *CVPR*, 2015. 1

[56] B. Yao, G. Bradski, and L. Fei-Fei. A codebook-free and annotation-free approach for fine-grained image categorization. In *CVPR*, 2012. 2

[57] B. Yao, A. Khosla, and L. Fei-Fei. Combining randomization and discrimination for fine-grained image categorization. In *CVPR*, 2011. 2

[58] N. Zhang, J. Donahue, R. Girshick, and T. Darrell. Part-Based R-CNNs for Fine-Grained Category Detection. In *ECCV*, 2014. 2, 4, 7

[59] N. Zhang, R. Farrell, and T. Darrell. Pose pooling kernels for sub-category recognition. In *CVPR*, 2012. 2

[60] N. Zhang, R. Farrell, F. Iandola, and T. Darrell. Deformable Part Descriptors for Fine-Grained Recognition and Attribute Prediction. In *ICCV*, 2013. 2

[61] N. Zhang, E. Shelhamer, Y. Gao, and T. Darrell. Fine-grained pose prediction, normalization, and recognition. *ICLR Workshops*, 2016. 2, 4, 6

[62] X. Zhang, H. Xiong, W. Zhou, W. Lin, and Q. Tian. Picking Deep Filter Responses for Fine-Grained Image Recognition. In *CVPR*, 2016. 7

[63] B. Zhao, X. Wu, J. Feng, Q. Peng, and S. Yan. Diversified Visual Attention Networks for Fine-Grained Object Classification. *IEEE Transactions on Multimedia*, 19(6):1245–1256, 6 2017. 3